Available online at www.sciencedirect.com
SCIENCE DIRECT
Journal of Power Sources 147 (2005) 214–219
JOURNAL OF POWER SOURCES
www.elsevier.com/locate/jpowsour

Structural and electrochemical properties of $(1-x)Li[Ni_{0.20}Li_{0.20}Mn_{0.60}]O_2$–$xLi[Co_{0.50}Li_{0.167}Mn_{0.333}]O_2$ for lithium secondary batteries

Young-Sik Hong [a,*], Yong Joon Park [a], Kwang Sun Ryu [a], Soon Ho Chang [a], Yu-Ju Shin [b,**]

[a] *Power Source Device Team, Electronics and Telecommunications Research Institute, Daejeon 305-350, Republic of Korea*
[b] *Department of Chemistry, Catholic University of Korea, Buchon 422-743, Kyeongki, Republic of Korea*

Received 18 October 2004; accepted 2 November 2004
Available online 20 July 2005

Abstract

$(1-x)Li[Ni_{0.20}Li_{0.20}Mn_{0.60}]O_2$–$xLi[Co_{0.50}Li_{0.167}Mn_{0.333}]O_2$ solid solutions ($x = 0$, 0.2, 0.4, 0.6, 0.8, and 1.0) have been prepared by a simple combustion method and investigated using X-ray diffraction (XRD), galvanostatic charge/discharge cycling, and cyclic voltammetry. The XRD analysis showed that single-phase compounds were obtained for all the compositions. Under the cycling condition of voltage range of 4.8–2.0 V and a specific current of 100 mA g^{-1} at 30 °C, the first discharge capacity was found to exhibit the maximum value of 265 mAh g^{-1} for $Li[Ni_{0.16}Co_{0.10}Li_{0.193}Mn_{0.547}]O_2$ ($x = 0.2$). Together with its excellent cycling property due to the structural stability, the observed capacity has potential for high capacity applications. It was also observed that the discharge capacity rapidly decreased during the cycling, when x is larger than 0.20. This implies that the charge/discharge mechanism of Ni-rich compounds is clearly different from that of Co-rich compounds, as being reflected in the evolution of cyclic voltammetry results.

Keywords: Lithium batteries; Cathode materials; Oxides

1. Introduction

The explosive demand for portable electronic devices has increased the importance of compact, lightweight, and reliable lithium secondary batteries, which consist of a transition metal oxide cathode and a graphite anode. Obviously, $LiCoO_2$ is an excellent cathode material with good reversibility and rate capability, but it suffers from high cost and the toxicity of cobalt. In this regard, olivine type and layered manganese-based materials are of high fundamental and technological interest as cathode alternative materials due to the low cost and toxicity [1–7]. Recently, Dahn et al. intensively attempted to stabilize the layered structure by using a solid solution between $Li[Li_{1/3}Mn_{2/3}]O_2$ and $LiMO_2$, such as $Li[Ni_xLi_{(1-2x)/3}Mn_{(2-x)/3}]O_2$, $Li[Co_xLi_{(1-x)/3}Mn_{(2-2x)/3}]O_2$, and $Li[Cr_xLi_{(1-x)/3}Mn_{(2-2x)/3}]O_2$ [3–6]. These results show that the electrochemically inactive $Li[Li_{1/3}Mn_{2/3}]O_2$ material can participate in the charge/discharge process when the $[Li_{1/3}Mn_{2/3}]$ is partially replaced by transition metal ions such as Ni^{2+}, Cr^{3+}, and Co^{3+}. In line with this, Ohzuku et al. tried to develop a layered $Li[Ni_{1/3}Co_{1/3}Mn_{1/3}]O_2$ system as a candidate material [7]. These compounds are described in the three-phase diagram consisting of $Li[Li_{1/3}Mn_{2/3}]O_2$–$Li[Ni_{1/2}Mn_{1/2}]O_2$–$LiCoO_2$, as illustrated in Fig. 1.

Very recently, we reported the structural and electrochemical properties of $Li[Ni_xLi_{(1-2x)/3}Mn_{(2-x)/3}]O_2$ and $Li[Co_xLi_{(1-x)/3}Mn_{(2-2x)/3}]O_2$ [8,9]. In view of high capacity, two compositions of $Li[Ni_{0.20}Li_{0.20}Mn_{0.60}]O_2$ and $Li[Co_{0.50}Li_{0.167}Mn_{0.333}]O_2$ exhibited the highest first discharge capacities of 288 mAh g^{-1} and 265 mAh g^{-1} at a

* Corresponding author. Tel.: +82 42 860 5057; fax: +82 42 860 6836.
** Co-corresponding author.
E-mail addresses: youngsik@etri.re.kr (Y.-S. Hong), yujushin@catholic.ac.kr (Y.-J. Shin).

0378-7753/$ – see front matter © 2005 Published by Elsevier B.V.
doi:10.1016/j.jpowsour.2004.11.018

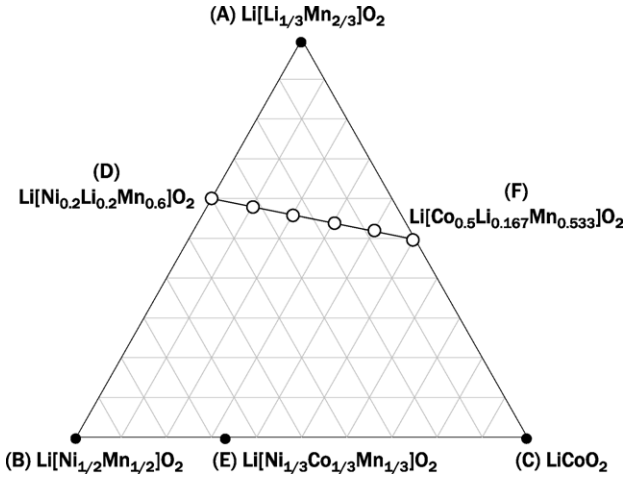

Fig. 1. Phase diagram of $Li[Li_{1/3}Mn_{2/3}]O_2$–$Li[Ni_{1/2}Mn_{1/2}]O_2$–$LiCoO_2$.

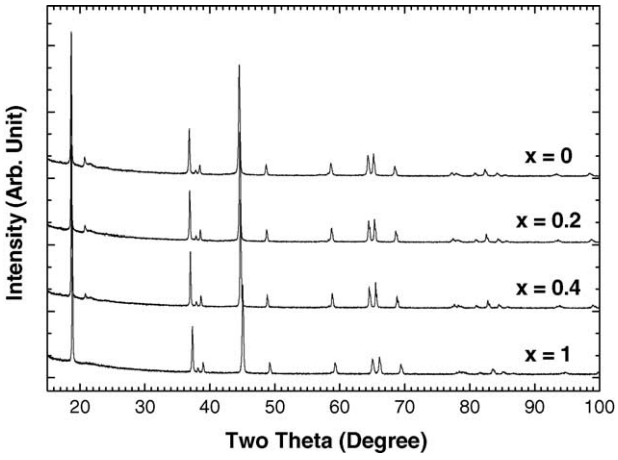

Fig. 2. Powder XRD patterns of $(1-x)Li[Ni_{0.20}Li_{0.20}Mn_{0.60}]O_2$–$xLi[Co_{0.50}Li_{0.167}Mn_{0.333}]O_2$ powders prepared at 900 °C for 5 h.

specific current of 20 mA g^{-1}, respectively. These two compounds have structural similarity to the pristine state, but displayed a totally different charge/discharge profile during the extended cycling: the former showed only a trivial structural variation while the latter experiences a transformation from a layered structure into spinel as the charge/discharge cycling proceeded.

In the present study, a simple combustion method is employed to prepare $(1-x)Li[Ni_{0.20}Li_{0.20}Mn_{0.60}]O_2$–$xLi[Co_{0.50}Li_{0.167}Mn_{0.333}]O_2$ solid solutions ($x = 0$, 0.2, 0.4, 0.6, 0.8, and 1.0). The obtained samples were investigated using XRD, galvanostatic charge/discharge cycler, and cyclic voltammetry. Their electrochemical properties have been discussed in relation to the structural evolution between Ni-rich ($x = 0$ and 0.2) and Co-rich compounds ($x = 0.4$, 0.6, 0.8, and 1).

2. Experimental

$(1-x)Li[Ni_{0.20}Li_{0.20}Mn_{0.60}]O_2$–$xLi[Co_{0.50}Li_{0.167}Mn_{0.333}]O_2$ ($x = 0$, 0.2, 0.4, 0.6, 0.8, and 1) powder was prepared by the simple combustion method, as reported in Ref. [8]. Firstly, the stoichiometric amounts of $Li(CH_3COO)\cdot 2H_2O$, $LiNO_3$, $Ni(NO_3)_2\cdot 6H_2O$, $Co(NO_3)_2\cdot 6H_2O$, $Co(CH_3COO)_2\cdot 4H_2O$, and $Mn(CH_3COO)_2\cdot 4H_2O$ (All chemicals were purchased from Aldrich Chem. Co.) were dissolved in distilled water and continuously stirred at 80 °C on a hot plate. The weight ratio of water to starting materials was about unity. To keep the combustion condition constantly, the molar ratio of acetate to nitrate was adjusted to 3:1. As the water evaporated, the mixed solution of Li–Ni–Co–Mn-(acetates, nitrates) turned into a viscous gel. It was directly fired at about 400 °C for 30 min in air. The decomposed powders were then heated at 900 °C for 5 h in air and quenched in a stainless steel plate. The heating rate of 100 °C h^{-1} was applied for all the temperature settings.

To investigate the crystal structure, we analyzed the as-prepared powders by XRD method using a Philips X'Pert Pro diffractometer equipped with a Cu target and the accumulative X-ray detector, X'Celerator. The scan data were collected in the 2θ range of 15–100°. All the XRD patterns were refined by the Rietveld method using the Fullprof program [10]. The peak shape was described by a pseudo-Voigt function. The background level was defined by a polynomial function. For each diffraction pattern, scale factor, counter zero point, peak asymmetry, and unit-cell dimensions were refined in addition to atomic parameters.

Electrochemical measurements were performed using a pouch-type cell, consisting of metal oxide cathodes and a lithium metal anode separated by a microporous polyethylene film. For the preparation of the cathode plate, 0.28 g PVdF was dissolved in about 10.5 g *N*-methyl-2-pyrrolidone for 1 h and then 3.4 g of the oxide powder and 0.32 g super P carbon black were added. After a day of ball-milling, the viscous slurry was coated on an aluminum foil (thickness = 15 μm) using a doctor blade and dried at 90 °C in a convection oven. The obtained cathode plate was dried at 120 °C for 2 h in a vacuum oven and then double roll pressed. Electrode sheets of 1.5 cm × 1.5 cm were cut from the plate. We used a 1 M $LiPF_6$ in a 50:50 mixture by volume of ethylene carbonate and dimethyl carbonate (Mitsubishi Chemical). The entire process was carried out in an environmentally controlled dry room. We measured the electrochemical properties using a Biologic Mac Pile II charge/discharge cycler at a voltage window of 4.8–2.0 V at 30 °C in a climatic test cabinet (Vötsch VC 7028). The cyclic voltammetry was conducted at a scan rate of 0.05 mV s^{-1}.

3. Results and discussion

Fig. 2 shows X-ray diffraction (XRD) patterns of $(1-x)Li[Ni_{0.20}Li_{0.20}Mn_{0.60}]O_2$–$xLi[Co_{0.50}Li_{0.167}Mn_{0.333}]O_2$

($x = 0$, 0.2, 0.4, and 1) samples prepared at 900 °C. Apart from the superlattice peaks appearing at $20° < 2\theta < 28°$, the diffraction peaks could be indexed based on O3-$LiCoO_2$ rhombohedral structure. The superlattice peaks has been considered to reflect the degree of ordering of cations in the 3b sites (referred as M-site) as observed in $Li[Li_{1/3}Mn_{2/3}]O_2$ [4]. Dahn et al. recently argued that the cations are partially arranged with degree of ordering in the M-site of $Li[Ni_xLi_{(1/3-2x/3)}Mn_{(2/3-x/3)}]O_2$, which can be regarded as "a true solid solution phase" [11]. On the other hand, a composite structure including nano-sized Li_2MnO_3-like phase was observed for $Li[Ni_xLi_{(1/3-2x/3)}Mn_{(2/3-x/3)}]O_2$, in which most of Li ions still participate in the electrochemical performance [12]. In both cases, the intensity of superlattce peaks, despite the interpretation being slightly different, can be regarded as a measure of ordering tendency at the M-site. Therefore, the weakening of those superlattice peaks with x indicates that the cations, such as Ni, Co, Li, and Mn at the M-site, are more homogeneously distributed as Co-content increases. The Co-rich phase $Li[Co_{0.50}Li_{0.167}Mn_{0.333}]O_2$ ($x = 1$) seems to relieve the charge-ordering tendency in the M-sites with respect to the Ni-rich phase $Li[Ni_{0.20}Li_{0.20}Mn_{0.60}]O_2$ ($x = 0$), resulting in a completely random distribution of the M-site cations.

A series of brief Rietveld analyses were performed to monitor the structural evolution with composition. For this reason, we adopted the high-symmetry space group of $R\bar{3}m$ (No. 166) rather than the low-symmetry monoclinic space group of $C2/m$ for a model structure. The profile analysis was doubly carried out for each composition on both conditions of including and excluding the superlattice peak region $20° < 2\theta < 30°$, respectively. The analysis reached to the minimum R_{wp} value when the site-exchange restrain of Ni^{2+} and Li^+ over the 3*a* and 3*b* sites as shown in Table 1. Such a site-exchange has been frequently occurred in layered oxide systems, mainly due to the similar ionic radii of Ni^{2+} (0.69 Å) and Li^+ (0.76 Å). The refinement gave good agreement factors of $R_{wp} = 14$–15% and $R_B = 3.5$–5.9% for all the compositions (in case of excluding the superlattice peak region). The contents of Ni^{2+} ions in the lithium layer were refined to around 2.8%, for $Li[Ni_{0.20}Li_{0.20}Mn_{0.60}]O_2$ ($x = 0$), resulting in the crystallographic composition of $[Li_{0.97}Ni_{0.03}]_{3a}[Ni_{0.17}Li_{0.23}Mn_{0.60}]_{3b}[O_2]_{6c}$. The occupancy of Ni^{2+} on 3*a* decreases sensitively to zero when x reaches to 0.40. This result is related to a decrease of Ni^{2+} content and shows a good consistency with the $LiNi_xCo_{1-2x}Mn_xO_2$ ($0 \le x \le 1/2$) system [13]. The variation of lattice parameters *a* and *c* is shown in Fig. 3. As Co-content is increased, both *a* and *c* are decreased. This can be attributed to the substitution of smaller Co^{3+} (0.545 Å) for Ni^{2+} (0.69 Å) ions. The *c*/*a* ratio increases from 4.99 to 5.01 with increasing Co content and indicates the increase of the two-dimensional layer properties. The smaller *c*/*a* ratio for Ni-rich phase is primarily due to the existence of Ni^{2+} ions at 3*a*. They should strongly attracts the adjacent MO_2, and slightly increase the 3D character.

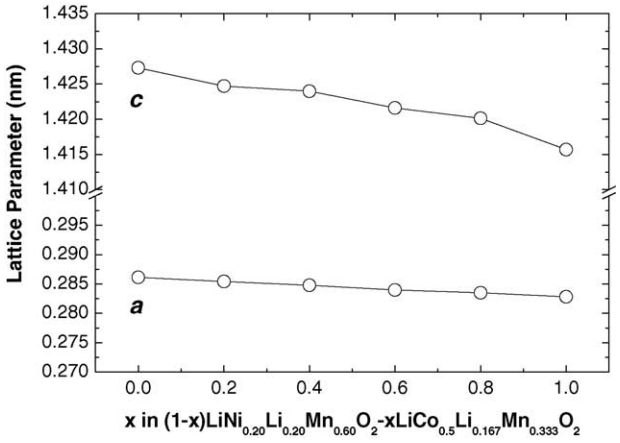

Fig. 3. The lattice parameters *a* and *c* of $(1-x)Li[Ni_{0.20}Li_{0.20}Mn_{0.60}]O_2$–$xLi[Co_{0.50}Li_{0.167}Mn_{0.333}]O_2$.

Fig. 4 shows the first charge/discharge voltage profiles of $(1-x)Li[Ni_{0.20}Li_{0.20}Mn_{0.60}]O_2$–$xLi[Co_{0.50}Li_{0.167}Mn_{0.333}]O_2$ ($x = 0$, 0.2, 0.4, and 1) cells cycled between 2.0 and 4.8 V at a constant specific current of 100 mA g^{-1} at 30 °C. All the cells exhibit long plateaus at around 4.5 V. Only the charge potential for the Co-free $Li[Ni_{0.20}Li_{0.20}Mn_{0.60}]O_2$ electrode showed a slightly higher value than the Co-substituted electrodes.

To investigate the difference more in detail, cyclic voltammetry was monitored at the range of 4.8–2.0 V with a scan rate of 0.05 mV s^{-1} as shown in Fig. 5. The initial oxidation peaks for all electrodes appeared at two regions of 3.7–4.2 and 4.4–4.7 V, respectively. Among them, the $Li/LiNi_{0.20}Li_{0.20}Mn_{0.60}O_2$ electrode exhibits two well-separated oxidation peaks at 3.8 and 4.1 V, which can be indexed as $Ni^{2+/3+}$ and $Ni^{3+/4+}$, respectively [14]. It is interesting that when a small amount of Co^{3+} is introduced into the M-sites ($x = 0.2$), a single oxidation peak attributable to $Co^{3+/4+}$ replaces the nickel doublet around 4.0 V [15]. It implies that the Co^{3+} ions should serve a catalytic center

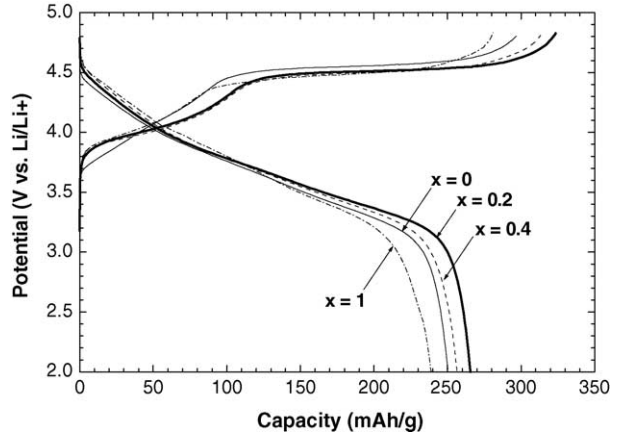

Fig. 4. First charge/discharge curves of $Li/(1-x)Li[Ni_{0.20}Li_{0.20}Mn_{0.60}]O_2$–$xLi[Co_{0.50}Li_{0.167}Mn_{0.333}]O_2$ cells cycled between 4.8 and 2.0 V at a constant specific current of 100 mA g^{-1}.

Table 1
Lattice parameters and R factors of $(1-x)$Li[$Ni_{0.20}Li_{0.20}Mn_{0.60}$]$O_2$–$x$Li[$Co_{0.50}Li_{0.167}Mn_{0.333}$]$O_2$

x	a (nm)	c (nm)	c/a	z (O)	Ni in 3a sites (%)	R_p (%)	R_{wp} (%)	R_B (%)
0	0.28611 (2)	1.4273 (2)	4.989	0.2435 (3)	2.8	18.3	15.2	5.90
0.2	0.28541 (2)	1.4247 (1)	4.992	0.2430 (3)	1.2	18.0	13.9	4.66
0.4	0.28479 (2)	1.4239 (1)	5.000	0.2424 (3)	0.1	19.2	14.6	4.11
0.6	0.28397 (2)	1.4216 (1)	5.006	0.2417 (3)	–	18.2	14.3	3.46
0.8	0.28348 (2)	1.4201 (1)	5.010	0.2410 (4)	–	18.9	14.1	3.71
1	0.28255 (2)	1.4160 (2)	5.013	0.2401 (3)	–	19.0	14.3	3.75

for the oxidation at this region: a small concentration of Co^{4+} ($t_{2g}^5e_g^0$) ions are firstly generated at the initial stage of oxidation, and then the ejected electrons from Ni^{2+} ions (which would run through the network -M-O-M-) can be temporarily 'trapped' into the stable t_{2g} orbital of Co^{4+}, and then completely dissociated from the matrix. It means that the oxidation peak of $Ni^{2+/3+}$ is merged into the peak of $Co^{3+/4+}$ and thus the observed single peak results from the superposition of two peaks of $Co^{3+/4+}$ and $Ni^{3+/4+}$.

The origin of the intense peak at around 4.5–4.65 V, being frequently observed in layered manganese oxides, has not been clearly understood up to now. It has been suggested that the peak is associated with the oxidation of Mn^{4+} to higher oxidation state, which acts as an oxidant and then gets back to Mn^{4+} ($t_{2g}^3e_g^0$) [4]. Actually this redox process is essential for generating the very large capacity of this kind of layered manganates, in that it induces a deep deintercation of Li ions from matrix. It should be noted that the oxidation potential of Mn^{4+} shifts toward to lower voltage region when the content of Co increases, as previously observed in Li[$Co_xLi_{(1/3-x/3)}Mn_{(2/3-2x/3)}$]$O_2$ [9]. An attempt to rationalize this phenomenon might be as following: Since Co^{4+} (t_{2g}^5) should be more electronegative than Mn^{4+} (t_{2g}^3), the electron density of O^{2-} should be more polarized toward Co^{4+} within the competitive bond Mn–O–Co. Consequently the energy level of Mn^{4+} in matrix should go up with Co-content because of the weakening of polarization effect [16] on Mn^{4+} by the coordinated O^{2-} ions, resulting in the decrease of oxidation potential of Mn^{4+}.

Fig. 6 shows the specific discharge capacity versus cycle number. All electrodes delivered an initial capacity over 240 mAh g^{-1}. Particularly, the Li/Li[$Ni_{0.16}Co_{0.10}Li_{0.193}Mn_{0.547}$]$O_2$ ($x = 0.2$) showed the highest capacity of 266 mAh g^{-1} with an excellent cyclability. As the Co-content increases from $x = 0$ to 0.2, the initial discharge capacities increase from 250 to 266 mAh g^{-1}, and then decrease to 244 mAh g^{-1} for $x = 1$. It is interesting that the Ni-rich electrodes ($x = 0$ and 0.2) show a good capacity retention and these exhibit a capacity above 215 mAh g^{-1} at 50th cycle. Meanwhile, the capacity of the Co-rich electrodes with $x > 0.4$ rapidly decreases with increasing cycle number. For example, the capacity of Li/Li[$Co_{0.50}Li_{0.167}Mn_{0.333}$]$O_2$ ($x = 1$) cell was abruptly decreased from 244 to 146 mAh g^{-1} at 50th cycle. This means that, during the charge/discharge, the electrochemical and structural evolution of Ni- and Co-rich electrodes is clearly different. Fig. 7 shows the 10 and 20th charge/discharge curves for the four electrodes ($x = 0$, 0.2, 0.4, and 1.0) cycled between 2.0 and 4.8 V at using a specific current of 40 mA g^{-1}. On discharge, there were distinct developments of 3 and 4 V plateaus for Li/Li[$Co_{0.50}Li_{0.167}Mn_{0.333}$]$O_2$ electrode. The 3 V plateau was certainly well developed as cycles proceeded. In fact,

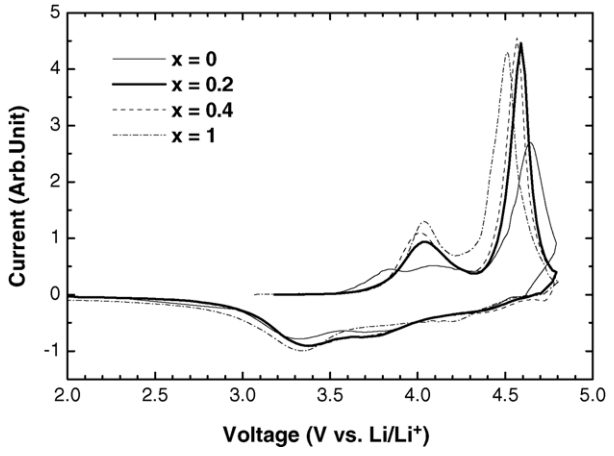

Fig. 5. Cyclic voltammograms of Li/$(1-x)$Li[$Ni_{0.20}Li_{0.20}Mn_{0.60}$]$O_2$–$x$Li[$Co_{0.50}Li_{0.167}Mn_{0.333}$]$O_2$ cells cycled between 4.8 and 2.0 V at a scan rate of 0.1 mV s^{-1}.

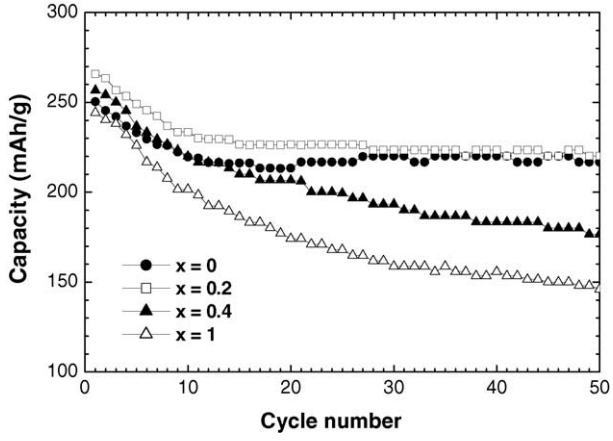

Fig. 6. Discharge capacity vs. number of cycles of Li/$(1-x)$Li[$Ni_{0.20}Li_{0.20}Mn_{0.60}$]$O_2$–$x$Li[$Co_{0.50}Li_{0.167}Mn_{0.333}$]$O_2$ cells cycled between 4.8 and 2.0 V at a constant specific current of 100 mA g^{-1}.

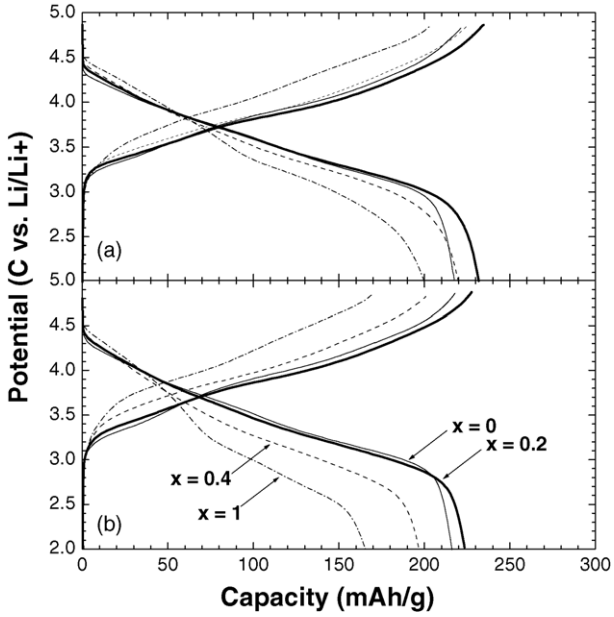

Fig. 7. (a) 10th and (b) 20th charge/discharge curves of Li/(1 − *x*)Li[$Ni_{0.20}Li_{0.20}Mn_{0.60}$]$O_2$–*x*Li[$Co_{0.50}Li_{0.167}Mn_{0.333}$]$O_2$ cells.

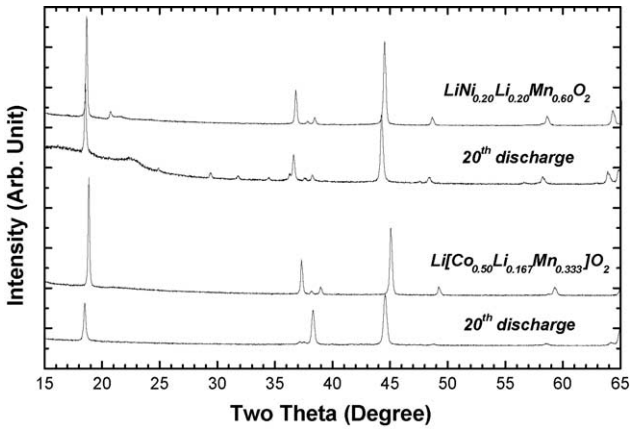

Fig. 8. Ex situ XRD patterns for the Li[$Ni_{0.20}Li_{0.20}Mn_{0.60}$]$O_2$ and Li[$Co_{0.50}Li_{0.167}Mn_{0.333}$]$O_2$ electrodes carried out at the end of 20th discharge.

such a voltage profile in Co-rich electrodes suggests the layered structure transforms into a spinel phase during the charge, as discussed in Li/Li_2MnO_3 electrode [17].

Fig. 8 shows an ex situ XRD analysis for the Li[$Ni_{0.20}Li_{0.20}Mn_{0.60}$]$O_2$ and Li[$Co_{0.50}Li_{0.167}Mn_{0.333}$]$O_2$ electrodes carried out at the end of 20th discharge. It is interesting that the XRD patterns of discharged Li[$Co_{0.50}Li_{0.167}Mn_{0.333}$]$O_2$ shows a big difference from its pristine compound, while those of discharged Li[$Ni_{0.20}Li_{0.20}Mn_{0.60}$]$O_2$ shows only a small 2θ shift to lower angles. It means that the crystal structure of Li[$Co_{0.50}Li_{0.167}Mn_{0.333}$]$O_2$ changes during the electrochemical cycling, resulting in the change of charge/discharge profiles (Fig. 7). It was reported that the crystal structure of Li_2MnO_3 transforms from the layered structure into a CrOOH-type P3 structure, via proton exchange mechanism during the charge [13]. The crystal structure of CrOOH is based on close-packed oxide ion layers stacked in an AABBCC sequence. That is, ex situ XRD measurements of discharged Li[$Co_{0.50}Li_{0.167}Mn_{0.333}$]$O_2$ show that its oxide packing was also changed from O3 to P3 stacking. In fact, the *c*/*a* ratio Li[$Co_{0.50}Li_{0.167}Mn_{0.333}$]$O_2$ is changed from 5.013 to 4.922 after the first charge, indicating the structural change as shown in Li_2MnO_3. Contrary to Li[$Co_{0.50}Li_{0.167}Mn_{0.333}$]$O_2$, the *c*/*a* ratio of Li[$Ni_{0.20}Li_{0.20}Mn_{0.60}$]$O_2$ are little changed. That is, the oxide ions keep their original ABCABC stacking sequence without any structural change. This may be due to a small amount of the Ni^{2+} ions located in the 3*a* sites as listed in Table 1, which play an important role as pillars between the transition metal layers. They prevent O3 stacking from gliding to P3 stacking. This is in agreement with the results of TEM and XRD in Li/Li[$Ni_{0.35}Li_{0.10}Mn_{0.55}$]$O_2$ [18].

In summary, we prepared (1 − *x*)Li[$Ni_{0.20}Li_{0.20}Mn_{0.60}$]$O_2$–*x*Li[$Co_{0.50}Li_{0.167}Mn_{0.333}$]$O_2$ solid solution and then tested their electrochemical and structural properties. The incorporation of a small amount of Co into Li[$Ni_{0.20}Li_{0.20}Mn_{0.60}$]$O_2$ improved its capacity, resulting in Li[$Ni_{0.16}Co_{0.10}Li_{0.193}Mn_{0.547}$]$O_2$ as the best composition. It seems, more interestingly, that the Ni^{2+} ions in the 3*a* sites stabilize the layered structure and contribute to a good cyclic performance.

Acknowledgement

This work was supported by the Ministry of Information and Communication of Korea in 2003.

References

[1] Y.-S. Hong, Y.J. Park, X. Wu, K.S. Ryu, S.H. Chang, Electrochem. Solid State Lett. 6 (2003) A166.
[2] Y.-S. Hong, K.S. Ryu, S.H. Chang, ETRI J. 25 (2003) 412.
[3] Z. Lu, D.D. MacNeil, J.R. Dahn, Electrochem. Solid State Lett. 4 (2001) A191.
[4] Z. Lu, L.Y. Beaulieu, R.A. Donaberger, C.L. Thomas, J.R. Dahn, J. Electrochem. Soc. 149 (2002) A778.
[5] D.D. MacNeil, Z. Lu, J.R. Dahn, J. Electrochem. Soc. 149 (2001) A1332.
[6] Z. Lu, Z. Chen, J.R. Dahn, Chem. Mater. 15 (2003) 3214.
[7] T. Ohzuku, Y. Makimura, Chem. Lett. (2001) 642.
[8] Y.-S. Hong, Y.J. Park, K.S. Ryu, S.H. Chang, M.K. Kim, J. Mater. Chem. 14 (2004) 1424.
[9] Y.J. Park, X. Wu, Y.-S. Hong, K.S. Ryu, S.H. Chang, J. Electrochem. Soc. 151 (2004) A720.
[10] J. Rodriguez-Carvajal, Program Fullprof, Version 3.2, January 1997, LLB JRC.
[11] Z. Lu, Z. Chen, J.R. Dahn, Chem. Mater. 15 (2003) 3214.
[12] W.S. Yoon, P. Paik, X.-Q. Yang, M. Balasubramanian, J. McBreen, C.P. Grey, Electrochem. Solid State Lett. 5 (2002) A263.

[13] D.D. MacNeil, Z. Lu, J.R. Dahn, J. Electrochem. Soc. 149 (10) (2002) A1332.
[14] J. Reed, G. Ceder, Electrochem. Solid State Lett. 5 (2002) A145.
[15] T. Ohzuku, A. Ueda, M. Nagayama, Y. Iwakoshi, H. Komori, Electrochim. Acta 38 (1993) 1159.
[16] P.A. Cox, Transition Metal Oxide: An Introduction to Their Electronic Structure and Properties, Oxford University Press, 1995.
[17] A.D. Robertson, P.G. Bruce, Chem. Mater. 15 (2003) 1984.
[18] J.-H. Kim, C.S. Yoon, Y.K. Sun, J. Electrochem. Soc. 150 (4) (2003) A538.